Available online at www.sciencedirect.com

ScienceDirect

Ceramics International 40 (2014) 3389–3398

CERAMICS INTERNATIONAL

www.elsevier.com/locate/ceramint

Fabrication and corrosion resistance of calcium phosphate glass-ceramic coated Mg alloy via a PEG assisted sol–gel method

Xuexin Wang[a], Shu Cai[a,*], Tielong Liu[b,**], Mengguo Ren[a], Kai Huang[a], Ruiyue Zhang[a], Huan Zhao[a]

[a]*Key Laboratory for Advanced Ceramics and Machining Technology of Ministry of Education, Tianjin University, Tianjin 300072, People's Republic of China*
[b]*Shanghai Changzheng Hospital, Shanghai 200003, People's Republic of China*

Received 13 September 2013; accepted 21 September 2013
Available online 27 September 2013

Abstract

To slow down the initial biodegradation rate of magnesium (Mg) alloy, crack-free $CaO–P_2O_5–SrO–Na_2O$ glass-ceramic coatings (CaPs) were synthesized using polyethylene glycol (PEG) assisted sol–gel method followed by a heat-treatment at 400 °C. The thermal behaviors of the synthesized glass-ceramics were characterized by differential scanning calorimetry and thermogravimetric (DSC/TG). The glass transition temperature (T_g) of calcium phosphate system shifted to a lower temperature (~226 °C) due to the addition of PEG, which promoted the crystal nuclei formation, thereafter induced a great amount of $Ca_2P_2O_7$ at a relatively low temperature. The effects of PEG addition on the corrosion behaviors of the coated Mg alloys were investigated by the electrochemical measurements and immersion tests in simulated body fluid (SBF). It was found that the coatings comprised of massive crystalline phases could slow down the degradation rate and decrease the mass loss of the Mg alloy substrates from 78.04% to 3.81% in the 7th day test, showing a better anti-corrosion property than that of the calcium phosphate coatings without the addition of PEG. Moreover, protection effect of PEG assisted synthesis of calcium phosphate coating gradually declined after the initial soaking time, which was confirmed by electrochemical impedance spectroscopy (EIS) analysis. These results implied that crystallization induced by PEG addition would affect the corrosion resistance of the coated Mg alloy and subsequently influence the degradation rate.

Keywords: A. Sol–gel processes; C. Corrosion; D. Glass ceramics; E. Biomedical applications

1. Introduction

Magnesium (Mg) and its alloys are highly potential for bioabsorbable/biodegradable orthopedic implants, such as bone fixation devices and scaffolds of artificial bone, because of their high specific strength, suitable density and low Young's modulus equivalent to that of human bone [1–4]. The ideal degradable biomedical implants are expected to be gradually dissolved, absorbed, or excreted in human body environment, and then disappear spontaneously after the tissue has healed sufficiently so that a second surgery to remove the implant could be avoided. However, the rapid degradation and limited bioactivity of magnesium alloy implants *in vivo* have prevented their widespread clinical applications [5–7]. The fast degradation rate in physiological environment, especially at the initial phase, usually results in a rapid reduction of mechanical support for the broken bone before the damaged bone healing. In addition, the rapid corrosion causes an abrupt pH increase, which may damage the neighboring tissues [3,5].

In this regard, some efforts have been made to slow down the biodegradation rate of Mg alloy, such as element alloying [8], purifying [9] and surface modification [6]. Surface modification such as protective coating on Mg alloys has been proven to be an effective way of controlling their initial degradation *in vivo* and maintaining desired mechanical properties [10,11]. In recent years, with the intent of reducing and controlling the corrosion rate and increasing the initial biocompatibility of Mg alloys, many researches focus on the development of bioactive coatings [12,13]. As bioactive coating materials, calcium phosphate glasses (CaPs) have been received considerable attentions as

*Corresponding author. Tel.: 86 22 2742 5069.
**Corresponding author. Tel.: 86 21 8188 6999.
E-mail addresses: caishu@tju.edu.cn (S. Cai), czyyltl@163.com (T. Liu).

0272-8842/$ - see front matter © 2013 Elsevier Ltd and Techna Group S.r.l. All rights reserved.
http://dx.doi.org/10.1016/j.ceramint.2013.09.093

hard tissue substitutes in biomedical field for several decades with regard to composition similarity and ability to spontaneously integrate with living bone by promptly forming bone-like apatite on the surface. Moreover, CaPs possess the low glass transition temperature and fabricating temperature, which can be controlled by adjusting the compositions of the glasses [14]. Such low fabricating temperatures of CaPs are well suited for preparing coatings on Mg alloys which have relatively low melting points of ~650 °C and poor heat resistance. Among these calcium phosphate glass systems, $CaO–P_2O_5–SrO–Na_2O$ glass has been studied as scaffold materials and confirmed to have good bioactivity and controlled degradability [15,16].

Many methods are known for preparing CaPs coatings on metallic substrates, especially on Ti alloys, such as wet chemical method, sol–gel method, plasma spraying method, *etc.* [12,17–19]. However, only a few of these techniques can be used to coat magnesium based alloys as most of these alloys are reactive to water based solutions and very sensitive to high temperature processes due to their low melting points. Roy et al. [12] prepared CaPs coating on Mg alloy using sol–gel method followed by a heat-treatment at 450 °C. The fabricating temperature of CaPs was about ~600 °C lower than that of the traditional melt-glass method (1000 °C–1050 °C) [20]. However, the CaPs present relatively high degradation rates in physiology environment, which is not beneficial for the corrosion protection of Mg alloys in the initial period. It has been reported that the crystallized phases derived from calcium phosphate glass matrix (such as calcium pyrophosphate and calcium metaphosphate) have lower degradation rates than the amorphous glasses [16,21]. It may suggest that increasing the amount of crystalline phases by heat-treatment of the glass matrix at a relatively low temperature is an essential step for the improvement of the corrosion resistance of the coated Mg alloys.

In this study, a new approach using polyethylene glycol (PEG) to promote crystallization of the sol–gel derived CaP glass-ceramic coating on Mg alloy at a relatively low temperature is explored. The effects of PEG on the composition and morphology of CaPs coating were characterized by X-ray diffraction (XRD), fourier transform infrared spectroscopy (FTIR) and field-emission scanning electron microscope (FE-SEM). The corrosion behaviors of the coated Mg alloys were studied by electrochemical method and immersion test in the simulated body fluid (SBF).

2. Materials and methods

2.1. Samples preparations

Commercial AZ31B magnesium alloy (the composition was shown in Table 1) substrates with dimensions of 10.0 mm × 10.0 mm × 2.0 mm were ground with SiC papers from 800, 1000, 1500 to 2000 grit, ultrasonically cleaned in ethanol for 10 min, and then dried in air.

The PEG assisted $CaO–P_2O_5–SrO–Na_2O$ calcium phosphate coatings (CaO 47%, P_2O_5 45%, SrO 2% and Na_2O 6%, based on mol%) (PEG–CaP) were synthesized by sol–gel and dip-coating method using P_2O_5 (Guangfu, Tianjin), $Ca(NO_3)_2 \cdot 4H_2O$ (Kermel, Tianjin), $NaNO_3$ (Kermel, Tianjin), $Sr(NO_3)_2$ (Damao, Tianjin) and PEG (Damao, Tianjin) as raw materials. The fabrication process of the phosphorous precursor was performed according to reference [22]. The solution containing network modifiers (Na_2O, CaO, and SrO) was prepared by dissolving corresponding salts ($NaNO_3$, $Ca(NO_3)_2 \cdot 4H_2O$, and $Sr(NO_3)_2$) into glycol successively. Subsequently, the solution was added drop wise to the phosphorous precursor and stirred vigorously to form a homogeneous solution. After addition of required amount of PEG (the concentration was 5 mmol/L), the pH of the mixture was adjusted to 6.0 using aqueous ammonia. Thereafter, coatings were deposited on Mg alloys via dip-coating technique with a withdrawal speed of 0.5 mm/s, and then aged at room temperature for 24 h and dried at 60 °C for 1 h. The coated samples were finally heat-treated at 400 °C for 2 h. For comparison, samples without PEG addition were also prepared (CaP). To avoid the influence of heat-treatment process, bare Mg alloy substrates were heat-treated at 400 °C under argon protection for 2 h and then were ground for characterization. Furthermore, to determine the thermal evolution and compositions of CaPs, corresponding powders of the two systems were synthesized through identical process without depositing on Mg alloy substrates.

Table 1
Chemical composition of AZ31B magnesium alloy (in wt%).

Al	Zn	Mn	Fe	Mg
3.0	1.0	0.2	< 0.005	Bal.

2.2. Characterization

Thermogravimetric (TG) and differential scanning calorimetry (DSC) analysis were performed using a NETZSCH, STA 499C device, at a constant heating rate of 5 °C/min up to 800 °C, in an alumina crucible and using 16 mg of xerogel. The surface morphologies of the glass-ceramic coatings before and after immersion were observed by FE-SEM (JEOL JSM-6700F, Japan). XRD (Rigaku, Japan) of prepared powders were performed employing Cu Kα radiation. Data were collected for 2θ ranging from 10° to 60°. Also, to investigate whether Mg alloy substrate affects the composition of the coating, low-angle (1°) XRD of CaP coated sample was performed. Furthermore, infrared absorption spectra of corresponding powders prepared through the same process were measured with a FTIR (Nicolet 5DX, USA).

2.3. Electrochemical tests

The corrosion resistances of the samples before and after being immersed in SBF for different periods were evaluated by means of potentiodynamic polarization test and electrochemical impedance spectroscopy (EIS) in SBF at 37 °C using the CHI660C electrochemistry workstation. A typical three-electrode cell with saturated calomel electrode (SCE) as the

reference electrode, platinum electrode as the counter electrode and the uncoated and coated Mg alloys as the working electrode was employed. SBF (pH = 7.40) was prepared according to Ref. [23]. The working electrode included an electrical connection wire, which was initially attached to the surface of the sample with conducting glue, leaving 1.0 cm^2 surface to expose in the electrolyte and the rest was sealed by epoxy resin. The samples were allowed to equilibrate for 10 min in SBF to reach a suitably stable open circuit potential before commencing the potentiodynamic polarization and EIS tests [24]. The potentiodynamic polarization tests were carried out at the scan rate of 1.0 mV/s. The electrochemical impedance spectra were measured at an open circuit potential with applied 10 mV sinusoidal perturbations and recorded using an excitation voltage of 32 mV root mean square over a frequency range from 100 kHz to 0.01 Hz.

2.4. Immersion tests

The immersion tests were carried out by soaking samples in SBF for different time using a WE-3 immersion oscillator. The volume of SBF used was based on a volume-to-sample area ratio 20 mL/cm^2, according to ASTM G31-72 [25]. The SBF was refreshed three days at a time during the immersion period. After the designated time, pH of each sample was measured by a pH meter (PHS-25, Leici, Shanghai). In order to evaluate the mass loss of uncoated and coated Mg alloy, specimens were removed from SBF, cleaned by chromic acid to remove the coatings and corrosion products [26], and then rinsed gently with anhydrous ethanol, cleaned ultrasonically in ethanol and dried in air. Thereafter, samples were weighted by means of an analytical balance. The mass loss was calculated as follows:

$$Mass\ \ loss = \frac{m_1 - m_0}{m_0} \times 100 \quad (1)$$

where m_0 is the sample mass before being immersed, m_1 is the mass of immersed sample cleaned by chromic acid. An average of five specimens was used for evaluating the mass variation. Immersed samples used for the surface observation were taken out without washing by chromic acid solution.

3. Results and discussion

3.1. Effect of PEG addition on the thermal behavior of the CaP glass

In order to study the effect of PEG addition on the thermal behavior of CaP glass and to determine an appropriate heat-treatment temperature, DSC/TG of CaP and PEG–CaP xerogels were performed and the results were shown in Fig. 1. The TG curves for both systems exhibited three stages of weight loss up to ~550 °C and then the weight remained constant in the later heating process. The first weight loss (less 5 wt%) occurred in the temperature range of room temperature to 180 °C could be ascribed to the loss of alcohol and water in the gel. This was verified by the endothermal peaks in the

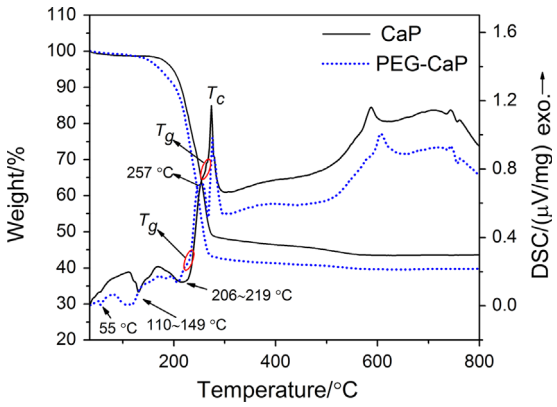

Fig. 1. DSC and TG curves of CaP and PEG–CaP xerogel powders.

range of 110–149 °C in both DSC curves. In addition, the endothermal peak at about ~55 °C for PEG–CaP sample might be associated with the dehydration reaction of PEG [27]. The second weight loss (~52 wt%) observed in the range of 180~280 °C could be associated with the partial elimination of organic residues (glycol), which was confirmed by the obvious endothermal peaks in the range of 206–219 °C for both systems. An extra exothermal peak at about ~257 °C for PEG–CaP xerogel could be ascribed to the decomposition of PEG to form CO_2 and H_2O [27]. The third weight loss occurred in the range of 280–550 °C was ascribed to the evaporation of residual alkyl phosphate.

Besides the above thermal peaks caused by the elimination of alcohol, water and organics, some characteristic peaks that were related with structural transformation and crystallization could also be observed in the DSC curves. Small endothermal peaks observed at ~260 °C for CaP and at ~226 °C for PEG–CaP samples might be attributed to the glass transition temperature (T_g) that represented the formation of the crystal nuclei. Clearly, T_g of the CaP glass shifted to a lower temperature due to the addition of PEG, indicating that the nucleation rate for PEG–CaP glass was higher than that for CaP. The exothermic signals at around ~276 °C for both systems were ascribed to the initiation of crystallization (T_c), which meant that the crystal nuclei began to grow rapidly if the glass was treated at ~276 °C. PEG–CaP glass with higher crystal nuclei rate would thus result in a larger amount of crystalline phases which will be confirmed in the following XRD tests.

On the basis of the above results, in order to obtain glass-ceramics with a relatively large amount of crystalline phases and in consideration of the poor heat resistance of Mg alloy substrate, 400 °C is chosen as the heat-treatment temperature for the coating preparation.

3.2. Phase compositions and glass structures of the glass-ceramics

To evaluate the effect of PEG on the crystallization behavior of CaP glass and to confirm that the glass-ceramic was formed on Mg alloy substrate, XRD of CaP powder, PEG–CaP powder and CaP coated sample were performed and the patterns were shown in Fig. 2. PDF#35-0821 is the standard

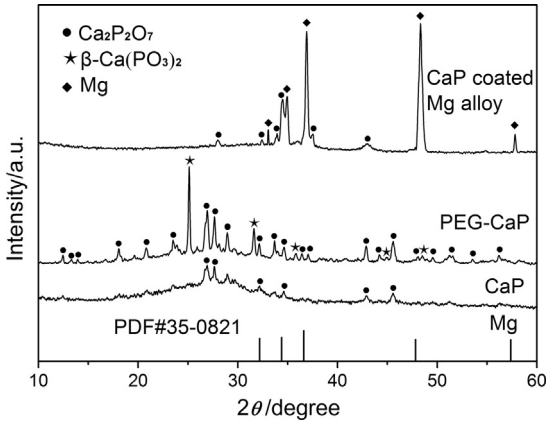

Fig. 2. X-ray diffraction patterns of CaP, PEG–CaP powders and CaP coated Mg alloy heat-treated at 400 °C.

pattern of Mg. The XRD patterns exhibited typical amorphous features. For CaP powder, only a small quantity of crystalline phases $Ca_2P_2O_7$ (JCPDS no. 09-0345) were detected. While for PEG–CaP sample, more $Ca_2P_2O_7$ and a few crystalline phases β-$Ca(PO_3)_2$ (JCPDS no. 09-0363) were detected after being heat-treated at the same temperature (400 °C), suggesting that the addition of PEG into the sol can promote the final crystallization of CaP system. For the coated sample, as the intensities of Mg peaks (according to the JCPDS card no. 35-0821) at $2\theta = 32.2°$, 34.4°, 36.6°, 47.8° and 57.4° were detected strongly, some peaks of $Ca_2P_2O_7$ were restrained and could not be detected. However, the diffraction pattern of $Ca_2P_2O_7$ was similar to that of the powder sample, and no new phase was observed beside the element of Mg, illustrating that the coatings have the same composition with the powders prepared by the same process and no reactions between the coatings and Mg alloy substrate occurred during the heat-treatment. Ultimately, the glass-ceramic was successfully formed on AZ31 Mg alloy.

In this study, alkyl phosphate was obtained by dissolving P_2O_5 in anhydrous ethanol [28]:

$$P_2O_5 + 3C_2H_5OH \rightarrow OP(OC_2H_5)(OH)_2 + OP(OC_2H_5)_2(OH) \quad (2)$$

$$2PO(OC_2H_5)_2(OH) \rightarrow (C_2H_5O)_2OP-O-PO(OC_2H_5)_2 + H_2O \quad (3)$$

The condensation shown in Eq. (3) resulted in the formation of gel with a three-dimensional network structure. The obtained gel, when being heat-treated at 400 °C, transformed to the finial protective coating which was composed of amorphous glass and a small amount of $Ca_2P_2O_7$.

However, when PEG was added to the sol, it might react with the monomers in Eq. (2). The reactions were as follows:

$$OP(OC_2H_5)(OH)_2 + HO(CH_2CH_2O)_nH \rightarrow OP(OC_2H_5)(OH)-O-(CH_2CH_2O)H + H_2O \quad (4)$$

$$OP(OC_2H_5)_2(OH) + HO(CH_2CH_2O)_nH \rightarrow OP(OC_2H_5)_2-O-(CH_2CH_2O)H + H_2O \quad (5)$$

According to Eqs. (4) and (5), PEG addition may suppress the condensation reaction (Eq. (3)) of forming the three-dimensional network to some extent and then affect the formation of glass network in the following heat-treatment process, resulting in a larger amount of crystalline phases.

For glass-ceramic coatings used in biomedical field, chemical durability in physiological environment is closely related to the dissolution of crystalline phases and residual amorphous glass. It has been reported that $Ca_2P_2O_7$ was stable and inert in distilled water [29]. And β-$Ca(PO_3)_2$ was proved to be extremely insoluble in aqueous solutions, even in acidified aqueous media [30]. Therefore, the corrosion resistance properties of the glass-ceramic coatings will mainly depend on the amount and structure of the residual glass matrix which will be characterized in the FTIR as shown in Fig. 3.

From the above XRD results, it can be concluded that the phase compositions of CaP coating and CaP powder were identical. Thus in order to avoid the interference of Mg alloy substrate, FTIR of CaP and PEG–CaP powders were conducted to investigate the influence of PEG on the glass structure. It can be seen from Fig. 3 that after PEG addition, the broad bands of the glass ceramic powder at around ~550 cm^{-1} and ~753 cm^{-1} were decomposed into several narrow peaks and the intensities of peaks for $(P_2O_7)^{4-}$ at 976–1050 cm^{-1} strengthened. The obvious peaks appeared in the region of 500–580, 650–800 and 930–1250 cm^{-1} corresponded to metaphosphate and pyrophosphate, $(PO_3)^-$ and $(P_2O_7)^{4-}$ [31], which were in accordance with functional groups of the crystalline phases identified by XRD results: $Ca_2P_2O_7$ and β-$Ca(PO_3)_2$. Except for these differences, the ν_{as} (P–O–P) and ν_s (P–O–P) at about ~900 cm^{-1} and ~753 cm^{-1}, and the ν_{as} (PO_2) at 1250–1300 cm^{-1} for both spectra indicated that the glass matrix had typical metaphosphate chain structure [28].

From XRD and FTIR results above, it can be inferred that with PEG addition, the structure of glass matrix did not changed while the amount of glass decreased. The metaphosphate chain structure mainly consists of Q^2 phosphate groups which have two bridge oxygen atoms, a non-bridge oxygen and a P=O double bond. Unlike silicon–oxygen tetrahedron

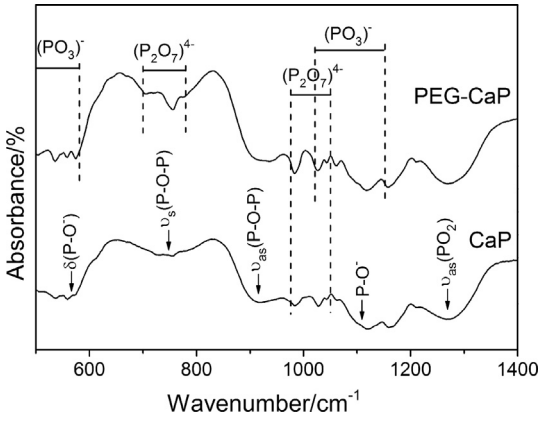

Fig. 3. Fourier transform infrared reflection spectra of CaP and PEG–CaP powders heat-treated at 400 °C.

[SiO_4], the Q^2 phosphate oxygen tetrahedron is not symmetrical owing to the difference between the P–O and P=O bonds, resulting in the relatively unstable property of phosphate glass [32]. Moreover, the non-bridge oxygen bonded with alkali or alkali earth cations in three-dimensional glass matrix is chemically active, which may induce ions exchange reactions between the cations and H^+ or H_3O^+ from solution easily [33]. The structure features and amorphous glass content may have a great impact on the corrosion resistance of the coating that will be discussed in the following EIS tests.

3.3. Effect of PEG on the surface morphology of the coating

The protection effect provided by the coating is also closely related to its surface morphology and microstructure. Thus to investigate the effect of PEG on the surface morphology and microstructure of CaP coating, FE-SEM for bare Mg alloy, Mg alloys coated with CaP and PEG assisted synthesis of CaP coatings were conducted and shown in Fig. 4. Low magnification SEM images of CaP and PEG–CaP coatings were similar, so the image of CaP coating was presented as a representative (Fig. 4b). From Fig. 4a, it can be seen that grinding scratches could be clearly detected on bare Mg alloy (Fig. 4a), while coated Mg alloys exhibited crack-free and continuous morphologies without any scratches (Fig. 4b), indicating that the substrates were fully coated with CaP glass-ceramics. SEM observations of CaP and PEG–CaP coatings at a high magnification exhibited obvious differences. For CaP coating containing mostly amorphous glass, the surface was smooth and homogeneous (Fig. 4c). However, PEG–CaP coating had a much rougher surface (Fig. 4d) due to the great crystallization from the glass matrix, which was verified by the XRD results.

3.4. Electrochemical characterization

Electrochemical tests including potentiodynamic polarization and EIS are the most commonly used techniques for studying the *in vitro* corrosion resistances of Mg alloys with or without coatings [34,35]. In this work, electrochemical tests were conducted to investigate the effect of PEG addition on the corrosion resistance of CaP coating and the results were shown in Fig. 5. For simplicity and comparison, the real impedance at which the imaginary part vanishes for the capacitive part, was approximately considered to be the charge transfer resistance (R_t), and regard it as a measure of corrosion resistance [36]. The estimated values of corrosion potential (E_{corr}), corrosion current density (i_{corr}) and R_t were derived and shown in Table 2. In general, the high R_t and low i_{corr} indicate that the test specimen has good corrosion resistance. It could be seen clearly that the coated Mg alloys had lower i_{corr} and larger R_t than those of bare Mg alloy, revealing the enhanced corrosion resistances afforded by the coatings. Moreover, the i_{corr} for PEG–CaP coated Mg alloy was 0.42 μA cm^{-2} lower than that of CaP sample, demonstrating that PEG–CaP coating was more effective in preventing Mg alloy from fast corrosion in the initial immersion time. Also, the corrosion potential was 0.08 V higher than that of CaP coated sample. And EIS data from Nyquist plots revealed that the R_t value increased from about 2.52 kΩ cm^2 to about 3.49 kΩ cm^2. It is known that the capacitive loop in Nyquist diagram corresponds to the limit of charge transfer resistance, being related to the

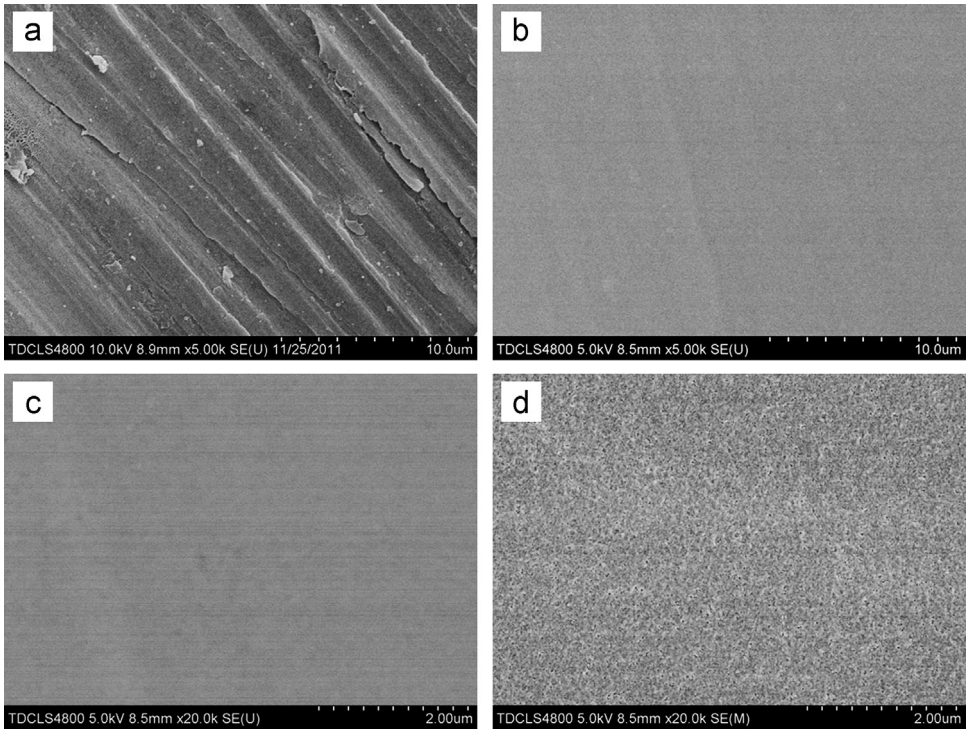

Fig. 4. FE-SEM images of surface morphologies of (a) bare Mg alloy, (b) CaP coated Mg alloy at a low magnification, and (c) CaP coated, (d) PEG–CaP coated Mg alloys at a high magnification.

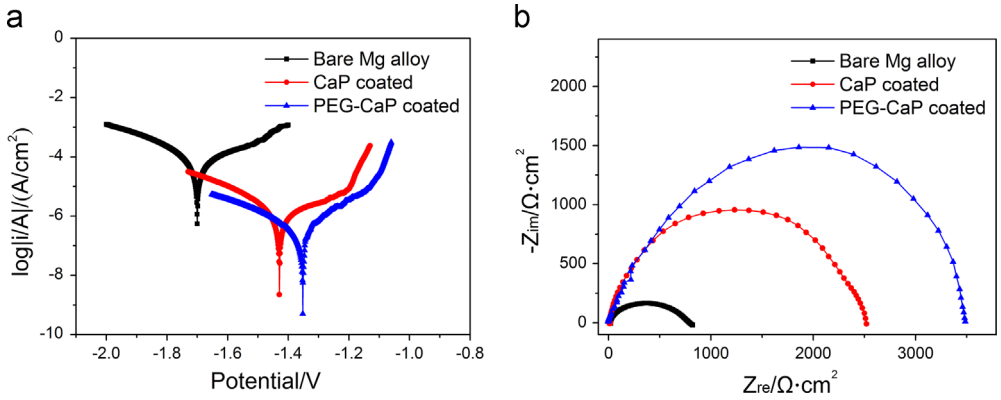

Fig. 5. (a) Potentiodynamic polarization curves and (b) Nyquist plots of bare Mg alloy, CaP and PEG–CaP coated Mg alloys.

Table 2
Corrosion properties of bare Mg alloy, CaP coated and PEG–CaP coated Mg alloys.

Samples	E_{corr} (V *vs.* SCE)	i_{corr} (μA cm^{-2})	R_t (kΩ cm^2)
AZ31 Mg alloy	−1.70	61.70	0.72
CaP coated	−1.43	0.55	2.52
PEG–CaP coated	−1.35	0.13	3.49

coating/electrolyte interface. With more charge transfer in the double electrode layer near the coating side, the resistance would be lower [37]. For CaP coating with more glass that contained Q^2 groups, the non-bridge oxygen atoms bonded with Na^+ or Ca^{2+} were chemically active, which might induce more charge transfer reactions that finally resulted in lower corrosion resistance. After adding PEG to the sol, crystallization from calcium phosphate glass matrix was promoted and thus the PEG–CaP coating with less amorphous glass had a larger charge transfer resistance as shown in the Nyquist plot above, suggesting that PEG–CaP coating could provide better protection for Mg alloy.

3.5. *Effect of PEG addition on in vitro corrosion resistance of CaP coating*

A proper range of local pH values can promote the osteoblast cell adhesion and proliferation, the apatite formation on the implant and the tissue growth *in vivo*. Additionally, the mass loss of the implant, especially in the early stage, affects its mechanical property that influences the healing of the damaged tissue. Therefore, the pH variations and mass loss for different samples in the *in vitro* immersion tests were examined and shown in Fig. 6. As shown in Fig. 6a, the slight pH decrease at the fourth and seventh days for all the specimens was due to the refreshment of the immersion media at the third and sixth days. It could be seen obviously that the coated samples exhibited much slower pH increase and mass loss owing to the well protection properties of the CaP glass-ceramics, and PEG–CaP coating showed better protective effect compared with CaP coating. After 3 days of immersion, the pH value and mass loss for bare Mg alloy reached 8.89 and 31.21% respectively, while those for the coated samples were in the range of 7.7–8.2 and 1.97%–4.23%, displaying much better corrosion resistances. It should be noted that pH value and mass loss for PEG–CaP coated Mg alloy were lower than those of CaP samples, suggesting that PEG–CaP coating could provide a better protection for Mg alloy substrates in SBF. Increasing the soaking time to 7 days, the PEG–CaP coated sample still kept the lowest pH value (7.59) and mass loss (3.81%), while those for CaP coated samples were 8.46 and 11.24% respectively. The pH value and mass loss for uncoated Mg alloy reached to a high value of 9.95 and 78.04% at the seventh day, indicating that bare Mg alloy suffered severe corrosion.

Macroscopic corrosion morphologies of bare Mg alloy, CaP coated and PEG–CaP coated Mg alloys after immersion in SBF for different periods were also observed and shown in Fig. 7. Aiming to compare the surface integrities of CaP coated and PEG–CaP coated Mg alloys, the samples were just cleaned with distilled water other than chromic acid. Before immersion, the bare Mg alloy presented a bright silver surface while the coated samples exhibited uniform and gray appearance due to the presence of the coatings. The bare Mg alloy suffered much more severe corrosion than the coated samples in the process of the whole immersion period, indicating that the coatings could provide effective protection for the Mg alloy substrates. After one day of immersion, there was minor corrosion on the surface of CaP coating, while the surface of PEG–CaP coated sample maintained uniform without any corrosion signs. After immersion for 3 days, the PEG–CaP coating still kept integrity without obvious corrosion, whereas some filiform corrosion could be detected for CaP coating. Continuing to extend the immersion time to 7 days, the PEG–CaP coating only exhibited minor corrosion. However, the surface of CaP coating showed more filiform corrosion and even some pits can be observed on the surface of the coating.

In general, the rapid corrosion of bare Mg alloy in corrosive medium is mainly ascribed to chemical dissolution while the corrosion behavior of the coated samples is related with the surface morphology and composition of the glass-ceramic coatings. Bare Mg alloy immersed in SBF usually suffers a rapid corrosion rate, depositing magnesium hydroxide dominant

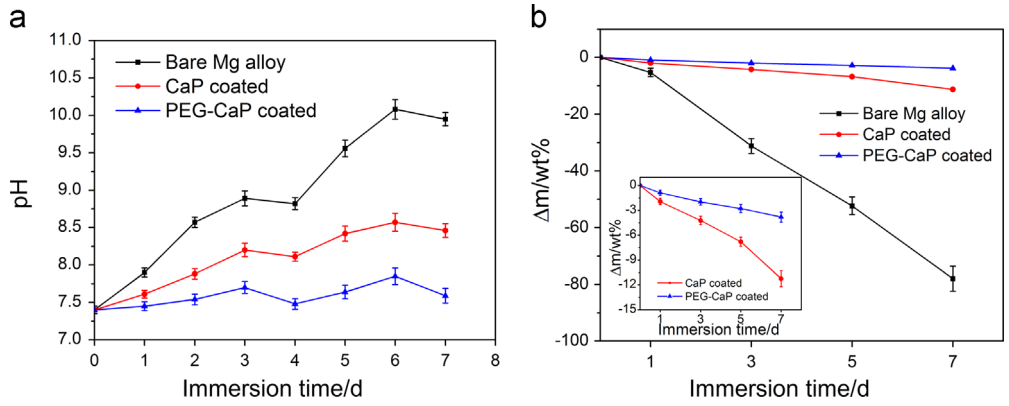

Fig. 6. pH variations and mass loss of bare Mg alloy, CaP coated and PEG–CaP coated specimens immersed in SBF for different periods. Inset in (b) shows the enlarged mass loss of CaP coated and PEG–CaP coated samples soaking in SBF for different periods.

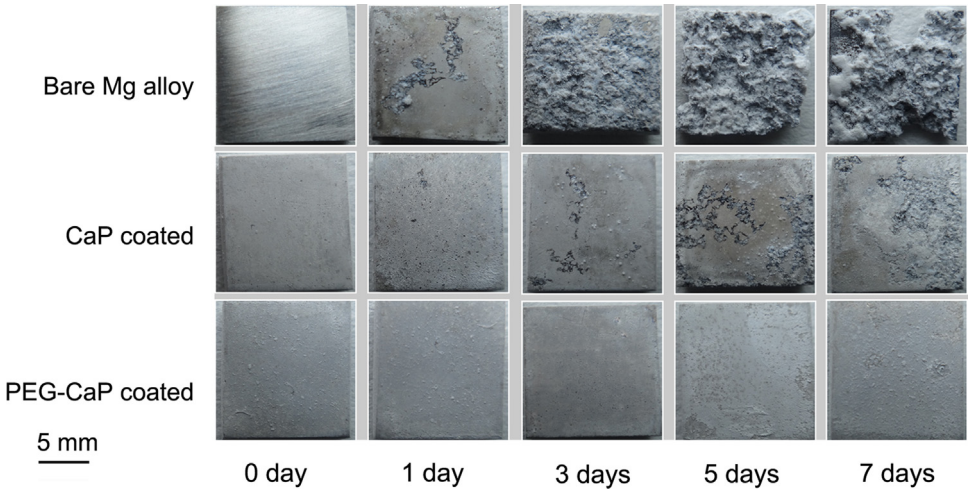

Fig. 7. Macroscopic corrosion morphologies of bare Mg alloy, CaP coated and PEG–CaP coated Mg alloys after being immersed in SBF for different periods.

corrosion product on the surface. Magnesium hydroxide will further react with chloride ions in SBF to form the soluble magnesium chloride as shown in Eq. (6) [38]:

$$Mg(OH)_2 + 2Cl^- \rightarrow MgCl_2 + 2OH^- \quad (6)$$

Therefore, the chemical dissolution of Mg would lead to the weight loss of the substrate and pH increase of the immersion medium. Also, the rapid corrosion would result in fast loss of bulk integrity as shown in Fig. 7. Nevertheless, for the coated samples, CaP glass-ceramics could act as effective physical barriers between the substrates and corrosion media, preventing Mg alloys from fast corrosion. Furthermore, as presented in Fig. 4, both coatings were crack-free and homogenous before immersion. Thus, the composition difference between CaP and PEG–CaP coatings played a more important role in the anti-corrosion behavior, which can be explained by the following EIS results.

3.6. Corrosion behaviors of the coated Mg alloys

To further compare the corrosion behaviors of CaP coated and PEG–CaP coated Mg alloys, EIS tests of the samples after immersion in SBF for three and seven days were conducted and the corresponding Nyquist plots were shown in Fig. 8. The obvious shrunken capacitive loops indicated that the corrosion protection abilities provided by the coatings decreased with the extension of immersion time. For CaP coated sample, the plots at 3 and 7 days (shown in Fig. 8a) could be divided by three well-defined loops: a high frequency capacitive loop which was related to the charge transfer reaction in the electric double layer formed at the interface between the sample surface and corrosion medium, a medium frequency capacitive loop that was attributed to the mass transfer in corrosion products layer and a low frequency inductive loop which was associated with the occurrence of pitting corrosion [39]. However, for PEG–CaP coated Mg alloy, the inductive loop in low frequency was only observed after being immersed in SBF for 14 days. And the resistance values were larger than those of CaP coated sample after the same immersion periods, suggesting that CaP coated Mg alloy suffered much severe corrosion as immersion time extended, which was consistent with the macroscopic surface morphologies shown in Fig. 7 and the FE-SEM observations presented in Fig. 9.

Fig. 9 showed the surface morphologies of CaP coated and PEG–CaP coated Mg alloys after immersing in SBF for three and seven days. After soaking 3 days, the CaP coating cracked severely (Fig. 9a) while PEG–CaP coating was still compact without any cracks (Fig. 9c). In literature, the erosion and

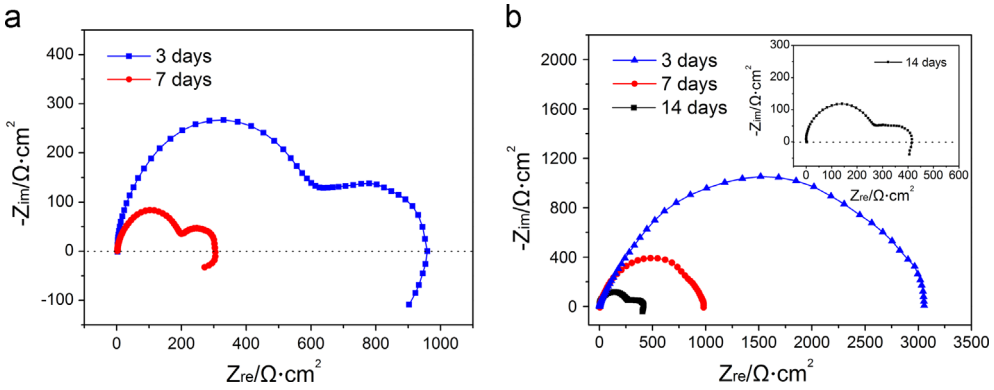

Fig. 8. Nyquist plots of (a) CaP coated and (b) PEG–CaP coated Mg alloys after immersion in SBF for different periods. Inset in (b) shows the enlarged EIS of PEG–CaP coated sample soaking in SBF for 14 days.

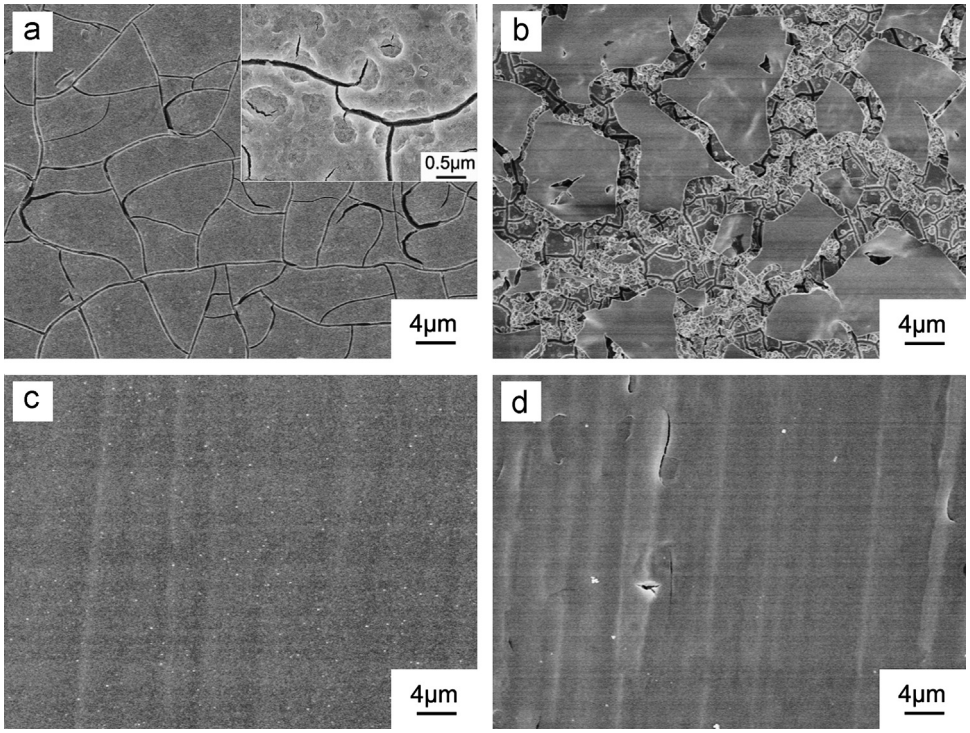

Fig. 9. FE-SEM images of surface morphologies of CaP coated Mg alloys immersed in SBF for (a) 3 days (the inset was the enlarged images); (b) 7 days; and PEG–CaP coated Mg alloys immersed in SBF for (c) 3 days; (d) 7 days.

abrasion effects of the flowing immersion media would lead to the decomposition of degradable coatings [40]. As the degradation rate of amorphous glass is much larger than that of the crystalline phases which has been demonstrated by previous studies, the amorphous glass in glass-ceramic coating would first degrade [16,21]. In this work, the CaP coating mainly consisted of amorphous glass and a small amount of crystalline phase $Ca_2P_2O_7$, while PEG–CaP coating contained less amorphous glass and more crystalline phases $Ca_2P_2O_7$ and β-$Ca(PO_3)_2$ (as analyzed in 3.2). The degradation of glass matrix in CaP coating resulted in concave and uneven surface, which caused the decrease of cohesion and led to cracks in the concave positions (inset in Fig. 9a). With further degradation, small cracks would extend and finally be connected (Fig. 9a). Once the surface cracked, the corrosive medium would contact directly with the Mg alloy substrate through these cracks and induce further corrosion, finally resulting in declined protection with the extension of immersion time (Fig. 8a). In comparison, PEG–CaP coating with more crystalline phases had a lower degradation rate, which ensured the integrity of the coating and provided effective protection for Mg alloy substrate. Increasing the immersion time to 7 days, more severe cracks and even partly peeling off from the substrate were observed in the CaP coating (Fig. 9b). Nevertheless, there was only a small amount of minor cracks detected for PEG–CaP coating (Fig. 9d), indicating that PEG–CaP coating can provide more effective protection for Mg alloy substrate than that of CaP coating.

4. Conclusion

To slow down the initial corrosion rate of magnesium alloy, homogenous and crack-free $CaO–P_2O_5–SrO–Na_2O$ glass-ceramic coating was successfully synthesized using PEG assisted sol-gel method. The glass transition temperature of calcium phosphate system shifted to a lower temperature (~226 °C) due to the addition of PEG, which promoted the crystal nuclei formation, thereafter induced crystallization ($Ca_2P_2O_7$) from glass matrix after heat-treated at 400 °C. The charge transfer resistance for PEG–CaP coated Mg alloy (3.49 kΩ cm^2) was much larger than that of CaP coated (2.52 kΩ cm^2) and uncoated (0.72 kΩ cm^2) Mg alloys, along with a more positive corrosion potential and a lower corrosion current density. Meanwhile, pH value and mass loss for PEG–CaP sample after being immersed in SBF for 7 days were 7.59 and 3.81% respectively, which were much lower than those for other samples, suggesting that PEG–CaP coating showed favorable protection for the magnesium alloy substrates in the initial period. With further increase of soaking time, the corrosion resistance of PEG–CaP coated Mg alloy gradually declined, making it to be a potential biodegradable material.

Acknowledgments

Authors acknowledge the financial support by National Nature Science Foundation of China (Grant no. 51372166, 81271954), Tianjin Science Foundation (Grant no. 11JCYBJC02600).

References

[1] M.P. Staiger, A.M. Pietak, J. Huadmai, G. Dias, Magnesium and its alloys as orthopedic biomaterials: a review, Biomaterials 27 (2006) 1728–1734.
[2] F. Witte, N. Hort, C. Vogt, S. Cohen, K.U. Kainer, R. Willumeit, F. Feyerabend, Degradable biomaterials based on magnesium corrosion, Current Opinion in Solid State and Materials Science 12 (2008) 63–72.
[3] G.L. Song, S.Z. Song, A possible biodegradable magnesium implant material, Advanced Engineering Materials 9 (2007) 298–302.
[4] Y. Xin, T. Hu, P.K. Chu, *In vitro* studies of biomedical magnesium alloys in a simulated physiological environment: a review, Acta Biomaterialia 7 (2011) 1452–1459.
[5] F. Witte, V. Kaese, H. Haferkamp, E. Switzer, A. Meyer-Lindenberg, C.J. Wirth, H. Windhagen, *In vivo* corrosion of four magnesium alloys and the associated bone response, Biomaterials 26 (2005) 3557–3563.
[6] H. Hornberger, S. Virtanen, A.R. Boccaccini, Biomedical coatings on magnesium alloys—a review, Acta Biomaterialia 8 (2012) 2442–2455.
[7] S. Shadanbaz, G.J. Dias, Calcium phosphate coatings on magnesium alloys for biomedical applications: a review, Acta Biomaterialia 8 (2012) 20–30.
[8] Y. Zong, G.Y. Yuan, X.B. Zhang, L. Mao, J.L. Niu, W.J. Ding, Comparison of biodegradable behaviors of AZ31 and Mg–Nd–Zn–Zr alloys in Hank's physiological solution, Materials Science and Engineering: B 177 (2012) 395–401.
[9] H.E. Boyer, T.Y. Gall, Metals handbook, Materials Park, American Society for Metals, Ohio, 1984, p. 8.
[10] A. Abdal-hay, N.A.M. Barakat, J.K. Lim, Hydroxyapatite-doped poly (lactic acid) porous film coating for enhanced bioactivity and corrosion behavior of AZ31 Mg alloy for orthopedic applications, Ceramics International 39 (2013) 183–195.
[11] D. Sreekanth, N. Rameshbabu, K. Venkateswarlu, Effect of various additives on morphology and corrosion behavior of ceramic coatings developed on AZ31 magnesium alloy by plasma electrolytic oxidation, Ceramics International 38 (2012) 4607–4615.
[12] A. Roy, S.S. Singh, M.K. Datta, B. Lee, J. Ohodnicki, P.N. Kumta, Novel sol–gel derived calcium phosphate coatings on Mg4Y alloy, Materials Science and Engineering: B 176 (2011) 1679–1689.
[13] D. Gopi, J. Indira, L. Kavitha, J.M.F. Ferreira, Hydroxyapatite coating on selectively passivated and sensitively polymer-protected surgical grade stainless steel, Journal of Applied Electrochemistry 43 (2013) 331–345.
[14] J.C. Knowles, I. Rehman, W. Bonfield, Spectroscopic and crystallographic analysis of the solution kinetics of a range of soluble phosphate based bioactive glasses, Bioceramics 7 (1994) 86–90.
[15] J. Massera, L. Petit, T. Cardinal, J.J. Videau, M. Hupa, L. Hupa, Thermal properties and surface reactivity in simulated body fluid of new strontium ion-containing phosphate glasses, Journal of Materials Science: Materials in Medicine 24 (2013) 1407–1416.
[16] J.X. Li, S. Cai, G.H. Xu, X.D. Li, W.J. Zhang, Z. Zhang, *In vitro* biocompatibility study of calcium phosphate glass ceramic scaffolds with different trace element doping, Materials Science and Engineering C 32 (2012) 356–363.
[17] H. Farnoush, A. Sadeghi, A.A. Bastami, F. Moztarzadeh, J. A. Mohandesi, An innovative fabrication of nano-HA coatings on Ti–CaP nanocomposite layer using a combination of friction stir processing and electrophoretic deposition, Ceramics International 39 (2013) 1477–1483.
[18] F. Batmanghelich, M. Ghorbani, Effect of pH and carbon nanotube content on the corrosion behavior of electrophoretically deposited chitosan–hydroxyapatite–carbon nanotube composite coatings, Ceramics International 39 (2013) 5393–5402.
[19] H. Farnoush, J.A. Mohandesi, D.H. Fatmehsari, F. Moztarzadeh, Modification of electrophoretically deposited nano-hydroxyapatite coatings by wire brushing on Ti–6Al–4V substrates, Ceramics International 38 (2012) 4885–4893.
[20] I. Ahmed, M. Lewis, I. Olsen, J.C. Knowles, Phosphate glasses for tissue engineering: Part 1. Processing and characterisation of a ternary-based $P_2O_5–CaO–Na_2O$ glass system, Biomaterials 25 (2004) 491–499.
[21] A.G. Dias, M.A. Lopes, I.R. Gibson, J.D. Santos, *In vitro* degradation studies of calcium phosphate glass ceramics prepared by controlled crystallization, Journal of Non-Crystalline Solids 330 (2003) 81–89.
[22] D. Carta, D.M. Pickup, J.C. Knowles, M.E. Smith, R.J. Newport, Sol–gel synthesis of the $P_2O_5–CaO–Na_2O–SiO_2$ system as a novel bioresorbable glass, Journal of Materials Chemistry 15 (2005) 2134–2140.
[23] T. Kokubo, H. Takadama, How useful is SBF in predicting *in vivo* bone bioactivity?, Biomaterials 27 (2006) 2907–2915
[24] N.T. Kirkland, N. Birbilis, J. Walker, T. Woodfield, G.J. Dias, M. P. Staiger, *In vitro* dissolution of magnesium–calcium binary alloys: clarifying the unique role of calcium additions in bioresorbable magnesium implant alloys, Journal of Biomedical Materials Research B: Applied Biomaterials 95B (2010) 91–100.
[25] ASTM Standard G31-72, Standard Practice for Laboratory Immersion Corrosion Testing of Metals, ASTM Standards, Philadelphia, PA, USA, 2004.
[26] K.Y. Chiu, M.H. Wong, F.T. Cheng, H.C. Man, Characterization and corrosion studies of fluoride conversion coating on degradable Mg implants, Surface and Coatings Technology 202 (2007) 590–598.
[27] J.L. Sun, L.F. Jiao, X. Wei, W.X. Peng, L. Liu, H.T. Yuan, Effect of PEG molecular weight on the crystal structure and electrochemical performance of LiV_3O_8, Journal of Solid State Electrochemistry 14 (2010) 615–619.
[28] D. Carta, J.C. Knowles, M.E. Smith, R.J. Newport, Synthesis and structural characterization of $P_2O_5–CaO–Na_2O$ sol–gel materials, Journal of Non-Crystalline Solids 353 (2007) 1141–1149.
[29] F.H. Lin, C.J. Liao, K.S. Chen, J.S. Sun, H.C. Liu, Degradation behaviour of a new bioceramic: $Ca_2P_2O_7$ with addition of $Na_4P_2O_7 \cdot 10H_2O$, Biomaterials 18 (1997) 915–921.
[30] J.M. Antonucci, B.O. Fowler, S. Venz, Filler systems based on calcium metaphosphates, Dental Materials 7 (1991) 124–129.
[31] S. Cai, W.J. Zhang, G.H. Xu, J.Y. Li, D.M. Wang, W. Jiang, Microstructural characteristics and crystallization of $CaO–P_2O_5–Na_2O–ZnO$

glass ceramics prepared by sol–gel method, Journal of Non-Crystalline Solids 355 (2009) 273–279.
[32] P.E. Gray, L.C. Klein, Chemical durability of sodium ultraphosphate glasses, Glass Technology 24 (1983) 202–206.
[33] O. Peitl, E.D. Zanotto, L.L. Hench, Highly bioactive P_2O_5–Na_2O–CaO–SiO_2 glass-ceramics, Journal of Non-Crystalline Solids 292 (2001) 115–126.
[34] N.T. Kirkland, N. Birbilis, M.P. Staiger, Assessing the corrosion of biodegradable magnesium implants: a critical review of current methodologies and their limitations, Acta Biomaterialia 8 (2012) 925–936.
[35] A.J. López, E. Otero, J. Rams, Sol–gel silica coatings on ZE41 magnesium alloy for corrosion protection, Surface and Coatings Technology 205 (2010) 2375–2385.
[36] I. Epelboin, C. Gabrielli, M. Keddam, H. Takenouti, Alternating-current impedance measurements applied to corrosion studies and corrosion-rate determination, in: F. Mansfeld, U. Bertocci (Eds.), Electrochemical Corrosion Testing, ASTM STP 727, ASTM, 1981, pp. 150–166.
[37] C. Alonso, J.A. Del Valle, M. Gamero, M. Fernández, Lorenzo de Mele, Do phosphate ions affect the biodegradation rate of fluoride-treated Mg?, Materials Letters 68 (2012) 149–152
[38] G. Song, A. Atrens, D. John St., X. Wu, J. Nairn, The anodic dissolution of magnesium in chloride and sulphate solutions, Corrosion Science 39 (1997) 1981–2004.
[39] M. Jamesh, S. Kumar, T.S.N. Sankara Narayanan, Corrosion behavior of commercially pure Mg and ZM21 Mg alloy in Ringer's solution-long term evaluation by EIS, Corrosion Science 53 (2011) 645–654.
[40] R.Z. LeGeros, Biodegradation and bioresorption of calcium phosphate ceramics, Clinical Materials 14 (1993) 65–88.